Semiempirical Model of Vibrational Relaxation for Estimating Absolute Rate Coefficients†

Scott H. Kable*

School of Chemistry, University of Sydney, Sydney, NSW, 2006 Australia

Alan E. W. Knight*

Molecular Dynamics Laboratory, School of Science, Griffith University, Brisbane, QLD, 4111 Australia

Received: May 30, 2003; In Final Form: September 29, 2003

A semiempirical theoretical model is developed for estimating the rates of collision-induced V−T vibrational relaxation from an initially excited vibrational state in a polyatomic molecule to a relatively dense field of destination vibrational states. The rationale has been to provide a means of estimating absolute relaxation rate coefficients, with a reasonable level of precision, for relaxation induced by a wide range of collision partners (atomic, diatomic, and polyatomic) and for a relatively wide range of temperatures. The model is based on calculating an efficiency *P* for the vibrational relaxation process by making use of relevant known molecular and intermolecular parameters. The inelastic rate coefficient for vibrational relaxation then emerges from a product of this efficiency and the classical Lennard-Jones elastic encounter rate. A feature of the model is that it uses no adjustable parameters. Comparisons are made between the predictions from the model and a number of experimental measurements of specific dependencies of vibrational relaxation rate coefficients (e.g. on collision partner properties, on the initial vibrational state, and on temperature) to characterize and illustrate the ingredients that deliver the estimate for *P*. A correlation between the predictions of the model and data from over 100 experimental systems and for a temperature range from 2−300 K invites the conclusion that the model is useful for estimating the absolute magnitude of state-to-field vibrational relaxation rate coefficients in the intermediate regime of final state densities to within an overall accuracy of 30% and with an average error of −10%.

I. Introduction

The exchange of vibrational, or thermal, energy between two interacting species is one of the most fundamental properties in chemistry and physics. This process is of course responsible for all thermal chemical reactions and the mechanisms by which systems return to equilibrium. Under ideal conditions (gas phase, small-molecule limit), the process can be followed at its most fundamental level—the transfer of population between individual quantum states of a molecule. When the density of states rises, it becomes more difficult to chart all destination states. However, the deactivation of a single quantum state can still be measured even when the background density of states is many thousand per wavenumber (intermediate case). Beyond this regime (large-molecule limit), when the individual states are poorly defined, the "states" become defined only by their energy, and the transfer process is defined by the average amount of energy transferred per collision.

The small-molecule and large-molecule limits have been the subject of extensive investigation, both theoretically and experimentally, for many decades.[1−10] Not only are the experimental measurements quite different between these regimes (state-to-state integral or differential cross section versus $|\Delta E|$), but the theoretical approaches are also quite disparate. Theories applied to the large-molecule regime are typically approximate and simple. They probably originate with Landau−Teller theory[11] through the Tanczos implementation[12] of Schwartz, Slawsky, and Herzfeld theory[13] (SSH/T) through a variety of other theories of varying complexity and accuracy.[14,15] In one of the most recent adaptations of SSH theory, Barker has shown that individual state-to-state processes can be integrated to provide a meaningful description of $|\Delta E|$ in the large-molecule limit at vibrational energies of tens of thousands of wavenumbers.[16]

Another widely adopted approach to explore energy transfer in the large-molecule limit has been to perform classical or semiclassical trajectory calculations.[15] This approach has provided many interesting results and new concepts, for example, the concept of the "supercollision".[15] However, it is not clear whether inherent deficiencies in the method (for example, zero-point energy) can be overcome to generate further insights into energy transfer.

The problem of small-molecule inelastic scattering has always been a fertile testing ground for theory. As experiments have yielded more and more precise data, so too has quantum scattering theory been able to address more complex interactions. For example, Clary and co-workers[17] have addressed the challenge of using 3D quantum scattering calculations to estimate vibrational relaxation rates for molecules such as CO_2, D_2CO, C_2H_4, C_3H_6, and *p*-difluorobenzene induced by collisions with He atoms. A combination of coupled-channel methods with sudden approximations, together with an atom−molecule potential energy surface obtained from self-consistent field calculations, yields estimates for state-to-state vibrational relaxation rate coefficients that are in good agreement with experimental data.

† Part of the special issue "Charles S. Parmenter Festschrift".

* E-mail: s.kable@chem.usyd.edu.au; A.Knight@griffith.edu.au.

10.1021/jp035516u CCC: $25.00
Published on Web 11/15/2003

The intermediate case of vibrational relaxation has received much less attention theoretically. In general, it is too complex for quantum scattering calculations, but the still-measurable quantum nature makes the simpler theories or classical trajectories too insensitive. Older theories concerned with the small intermediate limit have also utilized SSH/T theory. For example, Tang and Parmenter (TP)[18] used a simplified version of SSH/T theory[19] to explain the trends in state-to-field rate coefficients in benzene across a variety of initial states and collision partners. The TP model, however, was shown to be not applicable in other systems of similar complexity (aniline and pyrazine) by Rice and co-workers,[20−22] who then proposed a different symmetry-based model to explain the trends in these molecules.[22] However, Parmenter et al. subsequently showed that this model did not work for *p*-difluorobenzene.[23]

There is a wide variety of experimental data on quantum state resolved vibrational relaxation for the intermediate case regime. The systems range from diatomics (which never reach the intermediate case in complexity) through small polyatomics (e.g., CH_4, $C_2H_2O_2$, H_2CO) and larger aromatic polyatomics (e.g., benzene, aniline, *p*-difluorobenzene). These data cover both the S_1 and S_0 electronic states, vibrational states with from 1 to 100 quanta, 0 to 10 000 cm^{-1} of energy, densities of destination vibrational states from $\sim$0 to $>200/cm^{-1}$, and collision partners ranging from He to *n*-C_6F_{14}. It is a challenge for any theory to make a quantitative connection with this compendium of accumulated data.

Theories and relationships concerning the vibrational relaxation process in the intermediate regime, for example, those mentioned above, appear to have their merit in rationalizing trends in the data. We summarize the features that are found to be common to these studies:

(i) The classical Lennard-Jones collision encounter rate has provided a means for rationalizing the temperature dependence of the vibrational relaxation process between room temperature and the ultracold supersonic free jet environment.[24−26]

(ii) Propensity rules, based on the SSH/T model for vibrational relaxation,[1,2] appear to explain the relative magnitudes of state-to-state vibrational relaxation rate coefficients satisfactorily.[19,23]

(iii) Many relationships provide a rationalization of the dependence of the vibrational relaxation rate coefficient on the collision partner. Relationships based on both the reduced mass and on the intermolecular potential well depth have been found to be appropriate.[3,4,27] To some extent, the identities of the chosen set of collision partners dictate which is more suitable.

In this paper, we explore the application of a semiempirical model for vibrational deactivation (i.e., state-to-field relaxation) based on trends that we have observed in numerous systems. The seeds of our ideas are contained in Tang and Parmenter's exploration of vibrational relaxation in S_1 benzene,[18] but the application here involves a wide survey of existing data for numerous systems and contains some novel features. The essence of the model is that it provides a quantitative connection between the calculation of state-to-state propensities and the evaluation of the total rates of vibrational deactivation. We shall see that the model can be used to estimate absolute vibrational relaxation rate coefficients (for vibration to translational (V−T) energy transfer) for polyatomic systems in both S_1 and S_0 electronic states, a wide variety of collision partners and target molecules, and a wide range of initial vibrational levels (in number of quanta and in energy). The experimental vibrational rate coefficients vary over nearly 4 orders of magnitude; the model predicts vibrational relaxation rate coefficients each to better than 30% in most cases.

II. Theory

A. Background Theory. In this section, we present a derivation of a statistical, semiempirical, semiclassical model for estimating the rates of vibrational-energy transfer. In the subsequent section, we will demonstrate by comparison with experimental data that the model is sufficiently sensitive to the most important elements of vibrational-energy transfer to enable the estimation of absolute rate constants for vibrational deactivation in many systems under a wide variety of conditions.

We start by considering the rate of collisional encounters (in molecular units, $cm^3\ s^{-1}$) between a target molecule and a collision partner,

$$k = \int \sigma(v)\, v\, f(v)\, \mathrm{d}v \tag{1}$$

where the velocity distribution, $f(v)$, can be anything that the environment dictates but is often the Maxwell−Boltzmann distribution. The collision cross section is defined as

$$\sigma(v) = 2\pi \int_0^\infty b(v)\, \mathrm{d}b \tag{2}$$

where b is the impact parameter. When the impact parameter is independent of velocity (or temperature) and the velocity distribution is Maxwell−Boltzmann, then eq 1 becomes

$$k(T) = \sigma \sqrt{\frac{8k_B T}{\pi \mu}} = \sigma \langle v \rangle \tag{3}$$

where μ is the reduced mass and k_B is the Boltzmann constant. $\langle v \rangle$ is the mean relative speed. If the cross section is for hard spheres, then we can define the hard sphere collision cross section for two dissimilar molecules:

$$k_{hs}(T) = \pi d^2 \langle v \rangle \tag{4}$$

where $\pi d^2 = \sigma_{hs}$ and $d = {}^1/_2(d_A + d_B)$. d_A and d_B are the hard sphere diameters of species A and B, which are experiencing the collision.

The calculated collision rate is sensitive to the choice of intermolecular potential and hence σ. Our focus here is on vibrational relaxation rates, and several experiments have demonstrated that the hard sphere potential is not always appropriate.[24,28−31] The Lennard-Jones (6, 12) potential has been demonstrated to contain the essential features required to model various trends in observed vibrational relaxation rates.[32−39] The Lennard-Jones cross section σ_{LJ} is related to the hard sphere cross section via the omega integral, $\Omega^{(2,2)^*}$:

$$\sigma_{LJ} = \sigma_{hs} \Omega^{(2,2)^*} \tag{5}$$

where $\Omega^{(2,2)^*}$ contains the temperature dependence of σ_{LJ}. The choice of $\Omega^{(2,2)^*}$ over other $\Omega^{(l,s)^*}$ integrals is to some extent arbitrary, but there is a precedent for its use.[32−40] In any case, the difference between the various forms of the $\Omega^{(l,s)^*}$ integrals is slight.[41] k_{LJ}, the Lennard-Jones collision encounter rate coefficient, may therefore be written as

$$k_{LJ} = k_{hs} \Omega^{(2,2)^*} = \pi d^2 \langle v \rangle \Omega^{(2,2)^*} \tag{6}$$

Vibrational relaxation experiments commonly yield measure-

ments for the thermally averaged relaxation rate, k_{if}, which is the rate of population transfer from an initial vibrational state $|i\rangle$ to a final state $|f\rangle$ during the course of a collision. It has been customary to interpret these rates in terms of an "effective cross section", $\langle\langle\sigma\rangle\rangle$:

$$\langle\langle\sigma\rangle\rangle = \frac{k_{if}}{\langle v\rangle} \tag{7}$$

The double brackets $\langle\langle\ \rangle\rangle$ are used to indicate that this effective cross section is not a true average cross section but rather the ratio of averages (which is not equal to the average of the ratios). $\langle\langle\sigma\rangle\rangle$ may be used to define a probability P that describes the efficiency of the vibrational relaxation process relative to a calculable elastic collision rate:

$$P_{\mathrm{hs}} = \frac{k_{if}}{k_{\mathrm{hs}}} = \frac{\langle\langle\sigma\rangle\rangle}{\sigma_{\mathrm{hs}}} \tag{8}$$

or, relative to the Lennard-Jones encounter rate,

$$P_{\mathrm{LJ}} = \frac{k_{if}}{k_{\mathrm{LJ}}} = \frac{\langle\langle\sigma\rangle\rangle}{\sigma_{\mathrm{LJ}}} \tag{9}$$

Equation 9 pertains to direct state-to-state processes (i.e., vibrational relaxation from a state $|i\rangle$ to a state $|f\rangle$). To obtain the probability or efficiency for the total deactivation of an initially prepared state $|i\rangle$, we merely need to sum eq 9 over all destination states:

$$P_i = \sum_f \frac{k_{if}}{k_{\mathrm{LJ}}} = \frac{k_i}{k_{\mathrm{LJ}}} \tag{10}$$

B. Development of the Model. Equation 10 serves as the starting point to develop our model of vibrational-energy transfer. Our objective is to find a simple means of estimating P. Because $k_{\mathrm{LJ}} = \sigma_{\mathrm{LJ}}\langle v\rangle$, eqs 9 and 10 may be re-expressed as

$$k_i = P\langle v\rangle\sigma_{\mathrm{LJ}} \tag{11}$$

The probability factor, P, depends on the properties of both the target molecule and the collision partner, including the vibrational-level structure in the target molecule (and if applicable, the collision partner), the reduced mass of the collision pair, and features of the intermolecular interaction that are not reproduced by the Lennard-Jones potential (e.g., anisotropy). The strategy we shall adopt is to propose that P may be approximated by a product of two factors, one, α, that depends on the properties of the collision partner (but is specific to a given target molecule) and another, β, that depends on the properties of the target molecule. Equation 11 is therefore written as

$$k_i = \alpha \times \beta \times \langle v\rangle\sigma_{\mathrm{LJ}} \tag{12}$$

An empirical estimate of α emerges from a survey of the relationship between vibrational relaxation efficiency and collision partner identity for a wide range of systems (see below). It appears that P correlates well with the cube root of the reduced mass for the collision pair:

$$\alpha = c_1 \times \mu^{1/3} \tag{13}$$

We do not require nor is it suggested that eq 13 expresses a relationship with any precise mechanistic significance. Indeed, there are numerous other empirical relationships that work fairly well in rationalizing the collision partner dependence of relaxation processes.[4,27] We have chosen the correlation with $\mu^{1/3}$ because it specifically excludes factors that are already taken into account by the well depth, ϵ, for the intermolecular interactions. (k_{LJ} is a function of ϵ.) Also, it is a single-parameter correlation and hence offers the advantage of simplicity. Finally, the correlation appears to give an approximately zero intercept for all of the systems that we have examined. There are precedents for such correlations involving μ^r, where the factor r is fractional, depending on the conditions under which measurements were conducted.[4]

The second parameter, β, is calculated explicitly for each vibrational state of the target molecule. The model presumes that β may be evaluated as the sum of propensities for relaxation from the initially prepared state $|i\rangle$ to each of the destination states $|f\rangle$. Our goal here is to seek a simple, relatively intuitive model rather than a sophisticated theoretical treatment. Therefore, we have chosen one of the simplest approximations—the empirical Parmenter and Tang (PT) rules—as a starting point.[19] The PT propensity rules are based on the SSH semiempirical theory[13] for vibrational relaxation (including contributions from Tanczos[12] and Miklav and Fischer[42]). The SSH model was simplified substantially by PT by removing all dependence on the collision partner, including collision mass, intermolecular potential, and temperature. The PT expression for the relative probability P_{if} for a state-to-state relaxation process contains only factors relating to the energy difference between the initial and final states, the degeneracy of the final state, and the total change in vibrational quantum numbers between the initial and final states.

The PT formalism proved successful in rationalizing the relative mode-to-mode propensities for vibrational relaxation into different destination states from a single initial state in S_1 benzene.[19] It was later extended by Tang and Parmenter (TP) to model the relative relaxation rates for state-to-field relaxation from a number of initial states in benzene.[18] The TP model has been found to be less successful in describing state-to-state propensities in aniline[20,21] and pyrazine.[22] We have found that with small modifications their model provides a reasonable rationalization of the trends observed in the state-to-field relaxation in S_0 *p*-difluorobenzene.[30]

The PT propensity rules are summarized as follows:

$$P_{if} \propto I(\Delta E) \times \prod_j |\langle v_j|Q_j|v_j \pm \Delta v_j\rangle|^2 \tag{14}$$

where i and f are the initial and final states as before. The v_j's are the quantum numbers for the vibrational modes ν_j that change following the relaxation event from $|i\rangle$ to $|f\rangle$, and Q_j is the appropriate term in the interaction potential. In the PT rules, the first factor, $I(\Delta E)$, took three forms depending on the size and sign of ΔE.[19] We simplify the rules by choosing to differentiate only between exoergic and endoergic transfer processes:

$$\text{(i) } I(\Delta E) = \exp(-0.01\Delta E) \tag{15}$$

for exoergic processes, whereas to satisfy microscopic reversibility

$$\text{(ii) } I(\Delta E) = \exp(-0.01\Delta E) \times \exp\left(-\frac{\Delta E}{k_{\mathrm{B}}T}\right) \tag{16}$$

for endoergic processes.

The matrix elements in the second factor of eq 14 are approximated by the scaling law

$$|\langle v_j|Q_j|v_j \pm \Delta v_j\rangle|^2 = z_j 10^{-|\Delta v_j|} \tag{17}$$

In this approximation, each additional change in quantum number reduces the matrix element by 10. For quantum number changes with the same Δv but different v, the z_j's are determined from the standard recursion relations for the harmonic oscillator vibrational matrix elements. These recursion relations relate the size of the matrix elements for any fixed Δv quantum change. For example, the matrix element for transfer involving a 1-quantum change from $v \rightarrow v - 1$ is related to the change from $1 \rightarrow 0$ by

$$\langle v|Q_j|v-1\rangle|^2 = |\langle 1|\sqrt{v}Q_j|0\rangle|^2 = v|\langle 1|Q_j|0\rangle|^2$$

Therefore, in this example, $z_j = v$ and

$$|\langle 1|Q_j|0\rangle|^2 = 10^{-|\Delta v|} = 0.1$$

Similar relations apply in the case of $\Delta v > 1$ matrix elements.[43]

We may now proceed to evaluate β. The total probability for the deactivation of $|i\rangle$ due to vibrational relaxation will be proportional to the expression obtained by summing eq 14 over all final states $|f\rangle$:

$$\beta \propto \sum_f P_{if} \tag{18}$$

or

$$\beta = c_2 \times S_f \tag{19}$$

where S_f represents the sum of propensities P_{if}. Thus, eq 12 now takes the form

$$k_i = c_1\mu^{1/3} \times c_2 S_f \times \langle v\rangle\sigma_{LJ}$$

$$k_i = c\mu^{1/3} S_f \times \langle v\rangle\sigma_{LJ} \tag{20}$$

where $c = c_1c_2$ is simply the combined proportionality constant with units such that the probability factor $c\mu^{1/3}S_f$ is dimensionless.

The choice of the magnitude for c could in principle be left as an adjustable parameter, but we expressly seek a model (for predicting absolute rate coefficients) with no adjustable parameters. As we establish in the following section, an appropriate "universal" choice for the magnitude of c may be derived by exploring the empirical correlation between P_i and the cube root of the reduced mass for the collision pair. For a representative range of collision partners and for k_i in standard units of cm^3 s^{-1} (molecule^{-1}), μ in atomic mass units (amu), $\langle v\rangle$ in cm s^{-1}, and σ_{LJ} in cm^2, it is found that c emerges to be approximately unity (with units of amu$^{-1/3}$). Furthermore, in applying the model, we find that setting $c = 1$ is applicable for a wide range of temperatures. Hence, with c set conveniently equal to unity, we obtain our final expression for the total absolute rate of vibrational deactivation from an initially prepared state $|i\rangle$, viz.,

$$k_i = S_f \times \mu^{1/3} \times \langle v\rangle \times \sigma_{hs}\Omega^{(2,2)*} \tag{21}$$

III. Comparison with Experimental Data

There is a considerable body of experimental vibrational relaxation data available in the existing literature. To examine the reliability of our model, we shall use eq 21 to estimate vibrational deactivation rate coefficients for comparison with these data. Standard units for k_i are cm^3 s^{-1}. Experimental results, however, have been reported not only as rate coefficients in a variety of units but also as effective cross sections, collision numbers, and collision efficiencies. We have converted these results where necessary into the appropriate units.

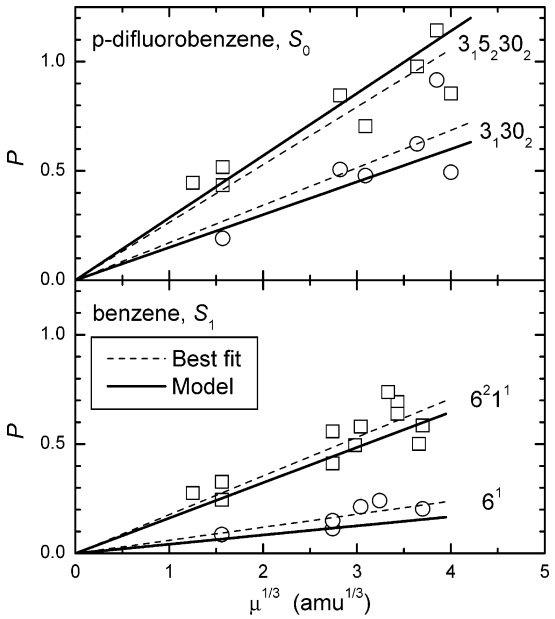

Figure 1. Correlation between probability factor $P = k_i/k_{LJ}$ and $\mu^{1/3}$ for (upper plot) S_0 pDFB[30] and (lower plot) S_1 benzene[19] and a variety of collision partners. In each case, the line of best fit is indicated by a dashed line, and the predictions of eq 21 are represented as a solid line.

The approach that we shall take is to examine each of the variables in turn. First, we demonstrate the validity of the $\mu^{1/3}$ and S_f factors and then explore the influences of temperature (collision energy), initial vibrational and electronic states, and target molecule complexity.

A. Collision Partner Dependence. In this section, we will demonstrate the applicability of the $\mu^{1/3}$ correlation contained in eq 21 using data relating to benzene and *p*-difluorobenzene (pDFB) prepared in a single vibrational level (i.e., a fixed S_f factor for each system). These molecules have featured centrally in the investigation of polyatomic vibrational relaxation, and data are available for a variety of initial levels and collision partners. The likely generality of this correlation is based on the data gathered for a representative variety of collision partners.

Figure 1 explores the correlation of P with $\mu^{1/3}$ in each system for two vibrational levels and a range of collision partners. The plot showing data for two vibrational levels in S_0 pDFB includes the collision partners He, H_2, D_2, N_2, SF_6, cyclohexane, and pDFB itself. For S_1 benzene, the collision partners are He, H_2, D_2, N_2, Ar, Kr, CO_2, CHF_3, C_2H_4, SF_6, and cyclohexane.

The correlation conforms reasonably well to a linear least-squares fit that is constrained to pass through the origin (dashed line) and supports the validity of the $\mu^{1/3}$ relationship at least for these data. A solid line, representing eq 21, is also drawn in Figure 1. This line tends to lie somewhat below the data. It may be tempting to reassign the constant c in eq 20 to a value larger than unity (a value of about 1.2 would be needed in Figure 1 to best overlap the dashed line with eq 21); however, we prefer to retain $c = 1$ for simplicity as well as to satisfy our intention to construct a useful model that works well enough with no adjustable parameters. Of course, additional relaxation processes

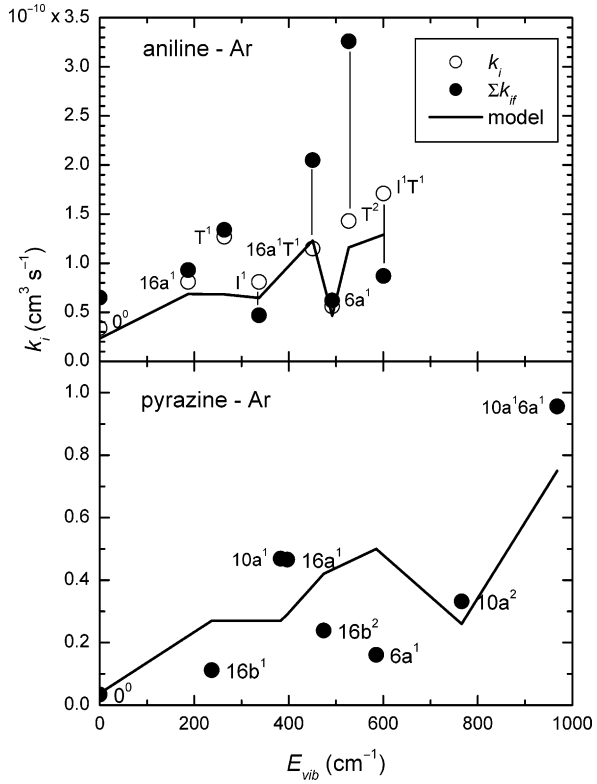

Figure 2. Plot of observed and predicted rate constant for vibrational relaxation by Ar for (upper plot) aniline[20] and (lower plot) pyrazine[22] in several vibrational states. In the case of aniline, two experimental measurements are available—a direct measurement of the rate constant indicated by open squares and a summation of individual state-to-state rate constants, as indicted by solid squares. The direct measurements are in better agreement with the model predictions.

(other than V−T) may be in operation for some collision partners. For example, points that lie substantially higher than the prediction in Figure 1 refer to polyatomic collision partners that might be expected to display V−T,R- or V−V-assisted vibrational relaxation.[44,45] The other smaller collision partners are, from our own experience and from other studies,[19,44] less likely to derive assistance from V−T,R or V−V mechanisms when acting as relaxation partners with S_1 benzene.

B. Vibrational-State Dependence of k_i. A range of data are available in the literature that permit an examination of how well the model predicts the dependence of k_i on the initially prepared vibrational state. We shall make use of vibrational relaxation data gathered for the four polyatomics—aniline, pyrazine, benzene, and pDFB—and incorporating a wide range of atomic, diatomic, and small polyatomic collision partners.

Aniline. Chernoff and Rice[20] (CR) explored vibrational relaxation pathways in S_1 ($^1B_2$) aniline for eight low-lying vibrational levels ($\epsilon_{vib} = 0-600$ cm^{-1}) using argon as a collision partner. They obtained rates for collision-induced population depletion of the initial state by two methods: (i) the direct measurement of k_i from the decay of fluorescence (this rate coefficient is labeled k_4 in the notation of CR) and (ii) by a summation of the individual state-to-state rate coefficients (labeled $k_i = \Sigma k_{if}$, which was labeled $\Sigma k_4(i)$ by CR). Figure 2a (upper plot) shows the measured rate coefficients for each vibrational level plotted as a function of vibrational energy. Two points are indicated for each vibrational level representing the estimate of k_i by each of the two techniques. The range of vibrational energies explored encompasses the lower part of the S_1 manifold (0−600 cm^{-1}). The "level" T^1 corresponds to excitation due to the band overlap of two states: $10b^1$ and 15^1. The rate displayed corresponds to the combined population decay of the two levels. In Figure 2a, we have plotted the data for the level "T" and its overtones and combinations at the midpoint of the energies of the states involved. Using the model (eq 21), we estimate the predicted rate coefficients for each vibrational level. These calculated rates are linked by an eye line in Figure 2a.

The two measurement techniques (decay of the initial state and sum of the growth rates) should ideally yield relaxation rate coefficients k_i and Σk_{if} that are equivalent. For cleanly excited levels (i.e., those not containing excitation in T), the two measurements by CR are in reasonable agreement (Figure 2a). However, for overtones and combinations involving the unresolved level T, this is not the case. For each of these grouped levels, the sum of the individual rate coefficients exceeds the total decay rate by roughly a factor of 2. This discrepancy between the two measurements of k_i was attributed by CR to systematic error in the original paper. We explore this issue a little further.

If one observes the population decay from a number of unresolved states, then the observed decay will be a population-weighted multiple exponential involving each of the individual decay rates. For example, if two unresolved channels have identical decay rates (for example, a 2-fold-degenerate vibration), then the observed decay rate is simply the decay rate that one would expect from cleanly exciting one of the components. In relation to the aniline data, our S_f factors identify that the two components of the T level ($10b^1$ and 15^1) should have similar decay rates, so the observed decay rate will be pseudo-exponential with a decay rate given approximately by the population-weighted mean of the two individual rates. Because we have no information concerning the population of each component of the coincidently excited initial states, we use both S_f factors equally to obtain the estimate for k_i (Figure 2a).

Figure 2a shows that eq 21 provides a good match with the directly measured rate coefficients k_i for vibrational relaxation induced by collisions with argon from each of the eight levels of aniline used by CR. The Σk_{if} estimates are scattered around the prediction line, thereby suggesting that the discrepancy between the two CR estimates of total relaxation rate coefficients may stem from greater errors in their measurements of state-to-state rate coefficients. As an absolute predictive instrument, eq 21 provides estimated rate coefficients that match the observed data for aniline−argon to within 20%, with a tendency to underestimate the observed values by ∼20%.

Pyrazine. McDonald and Rice[22] (MR) have used S_1 pyrazine ($C_4N_2H_4$) as a target for vibrational relaxation induced by collisions with argon. Their investigation was directed primarily at obtaining relative rates for mode-to-mode energy flow and led to the development of their correlation diagram model for state-to-state vibrational relaxation pathways. MR quote a variety of state-to-state relaxation rates for individual channels that may be converted into total vibrational relaxation rates by adding the rates of all identified channels. There are likely errors in this procedure, as identified above in the case of aniline, but the data still serve as a useful test of our model.

Figure 2b shows the experimental rate coefficients, together with rate coefficients derived using our model, plotted against the vibrational energy of the initial state. Figure 2b demonstrates that the magnitude of the estimated rates matches the observed rates fairly well. The observed rates lie above or below the predictions by ≤∼50%. However, the observed vibrational-state dependence now appears more poorly catered to by the model. This may be a shortcoming in the model or, as we believe,

simply uncertainty in the data caused by our summation of the individual state-to-state rate data to form state-to-field rates. The discrepancies seen in Figure 2b are in fact no worse than those seen in the data for aniline obtained from summed state-to-state rates.

Benzene: A Case Involving Degenerate Vibrations. Tang and Parmenter[18] used their original SSH-based propensity rules to investigate relative state-to-field vibrational relaxation rates in S_1 benzene colliding with CO. Our approach for modeling the dependence of k_i on the initially prepared vibrational state is based on their work, but we have introduced modifications that permit the estimation of the absolute magnitude of the vibrational relaxation rates. Furthermore, we find that the PT treatment for degenerate vibrations needs to be reinvestigated.

In the original PT formulation, the probability that a molecule will change its vibrational state during a collision was set proportional to the degeneracy of the final state g_f:

$$P(i \rightarrow f) = g_f P(i \rightarrow f_a) \tag{22}$$

where f_a is a single nondegenerate component of the final state. However, the PT formalism does not cater to instances where the initial state is also degenerate. We consider three examples relating to S_1 benzene vibrational relaxation: (i) relaxation from a nondegenerate state (e.g., 0^0); (ii) relaxation from a degenerate state (e.g. 6^1); and (iii) relaxation from an overtone of a degenerate state (e.g., 6^2).

(i) Relaxation from a Nondegenerate State. Consider the vibrational excitation channel $0^0 \rightarrow D^1$ where D is a degenerate mode. D contains the two vibrational angular momentum components (0, 1) and (1, 0). Because the two channels $0^0 \rightarrow D^{(0,1)}$ and $0^0 \rightarrow D^{(1,0)}$ will have identical propensities in the calculation of S_f, we predict that $P(0^0 \rightarrow D) = g_f \times P(0^0 \rightarrow D^{(0,1)})$, as espoused in the original PT formalism.[19]

(ii) Relaxation from a Degenerate State. When the initial state is degenerate, the case is different. In principle, it is equivalent to the situation described previously in relation to aniline where relaxation from two initial states could not be resolved: measurement of the combined decay of both of the unresolved states gives a decay rate that is a (population-weighted) linear combination of the decay of the individual states. For a degenerate level (e.g., for 6^1), the two components $6^{(1,0)}$ and $6^{(0,1)}$ have identical decay rates, so the measured decay rate is equal to the decay from either component. Assume for now that the two components are not coupled. For a particular degenerate destination channel, however, the propensity may differ for each component. This detail is not considered in the PT model; for example, the PT calculation would evaluate the propensity for $6^1 \rightarrow 6^1X^1$ as

$$P(6^1 \rightarrow 6^1X^1) = 2 \times P(6a^1 \rightarrow 6a^1X^1)$$

where $g_f = 2$ for nondegenerate X and $6a^1$ is treated as nondegenerate.

We believe that this formalism is incorrect. Certainly $6a^1 \rightarrow 6a^1X^1$ is a 1-quantum change involving ν_X, but $6a^1 \rightarrow 6b^1X^1$ is a 3-quantum change (loss of ν_{6a} and gain of ν_{6b} and ν_X). A 3-quantum change must be less favorable, and indeed the PT empirical factors suggest that it will occur with a 100-fold lower propensity than an equivalent 1-quantum change. Our approach, therefore, shall simply be to drop the degeneracy factor and instead include two levels 6a and 6b with the same frequency. By doing this, the $\Delta v = 1$ and $\Delta v = 3$ channels are automatically distinguished, and the correct propensity is evaluated. This procedure also applies for combinations of degenerate modes.

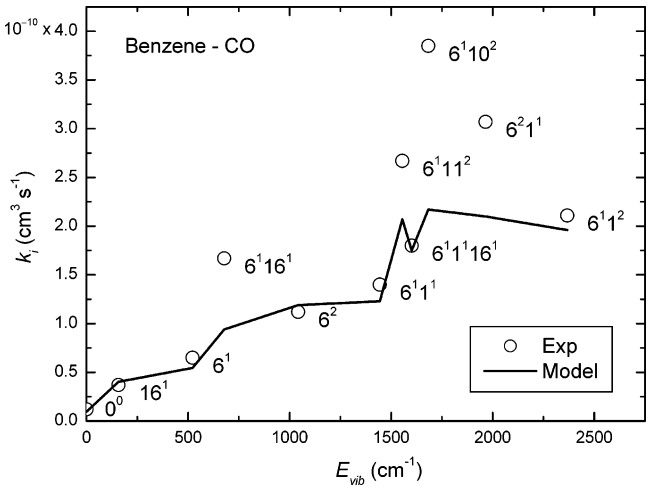

Figure 3. Vibrational-energy dependence of vibrational relaxation rate k_i for a variety of vibrational levels in S_1 benzene under collisional assault by CO.[18] Experimental data are represented by open circles. The solid line connects rate coefficients estimated by the model for each vibrational level.

If the two degenerate components are coupled (as they are in benzene), then the correct propensity may be calculated if the quantum mechanical coefficients of the mixing are known. For a two-state degenerate system, the state mixing coefficients are respectively $\pm(1/\sqrt{2})$. In fact, because the relaxation rates are contributed to equally by the sum of 1- and 3-quantum processes and hence should be equivalent for each degenerate component, the extent of mixing will not change the calculated rate.

(iii) Relaxation from Overtones of Degenerate Vibrations. Relaxation from the overtone of a degenerate mode (e.g., 6^2) can also be evaluated by distinguishing the degenerate states as 6a and 6b. Level 6^2 is of course 3-fold degenerate: $6a^2$, $6a^16b^1$, and $6b^2$. Each of the components $6a^2$ and $6b^2$ will display identical decay rates according to eq 21. However, the $6a^16b^1$ state may decay at a different rate. To compare with the experimental vibrational relaxation rate from 6^2, we must weight the propensities for each component by the population in each of the three states. For the coherent excitation of all components, the populations are equal, and we can weight our mean appropriately. If the decay rates are significantly different and/or the decay curves are measured sufficiently accurately and for a sufficiently long time, then the multiple-exponential behavior of the decay may be observed.

We have applied these rules for degenerate vibrations to the data of Tang and Parmenter.[18] They have measured vibrational deactivation rates for a number of S_1 vibrational levels in benzene. Included in these levels are nondegenerate species (e.g., 0^0), degenerate fundamentals (e.g., 6^1 and 16^1), combination bands of degenerate and nondegenerate levels (e.g., 6^11^1 and 6^11^2), combination bands of two degenerate modes (e.g., 6^1-16^1), degenerate overtones (e.g., 6^2), and degenerate and nondegenerate combinations of overtones (e.g., 6^110^2, 6^111^2, 6^21^1, and $6^116^11^1$). This set of data should provide a rigorous testing ground for our reformulation of the treatment for degenerate states.

The observed rate constants and the estimates deduced from our model for benzene vibrational relaxation induced by collisions with CO are displayed as a function of the vibrational energy of the initially prepared state in Figure 3. Estimated rate coefficients for the majority of levels are within ±20% of the observed data. The exceptions are the three levels 6^116^1, 6^110^2,

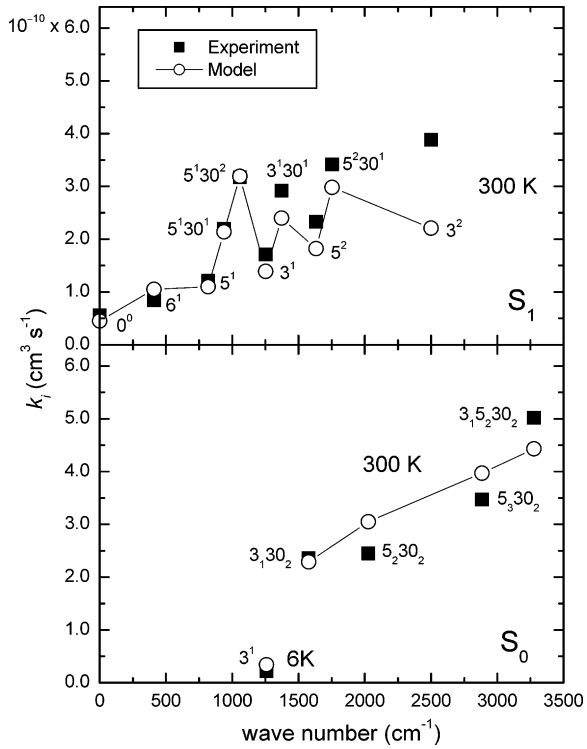

Figure 4. Vibrational-energy dependence of k_i in both S_0 (lower plot)[30] and S_1 (upper plot)[51] *p*-difluorobenzene. Experimental data are represented by solid symbols. The line connects rate coefficients estimated by the model (open circles) for each vibrational level.

and 6^21^1. Each of these levels is at least 3-fold degenerate. The worst fit is for the 6-fold-degenerate level 6^110^2. There may be a number of explanations for these discrepancies between observed and predicted rate coefficients.

First, we explore whether there are reasons that our treatment of degenerate vibrations may be incorrect. We have considered an equal population of the aa, ab, and bb components in levels involving either 6^2 or 10^2 and have weighted our S_f factors accordingly. We have also ignored any coupling between the components. It turns out that the ab level has a very similar S_f factor to that for the other components of 6^2 or 10^2, so the population weighting and coupling are unimportant in any case. In support of our treatment, the match between observed and estimated rates for levels 6^2 and $6^116^11^1$ is excellent (Figure 4). We therefore ask why the estimated and observed rate coefficients are equivalent for these 3-fold degenerate levels whereas the model does not work so well for 6^116^1, 6^21^1, and notably 6^110^2. A closer examination of some of these levels that display aberrant behavior is warranted.

Level 6^116^1 relaxes vibrationally with a rate coefficient that is substantially faster than that estimated using eq 21. All other levels involving the ν_{16} vibration, however, are modeled quite adequately. The observed rate coefficient for this level (1.67×10^{-10} cm^3 molecule^{-1} s^{-1}) is only fractionally below that for level $6^116^11^1$ (1.80×10^{-10} cm^3 molecule^{-1} s^{-1}), which lies some 1000 cm^{-1} higher in energy and contains the additional vibrational mode ν_1 in its character. The addition of extra modes in a vibrational description has been observed to increase the vibrational relaxation rate substantially. (See, for example, levels 5_230_2 and $3_15_230_2$ in S_0 pDFB[30] or the addition of a single quantum of ν_{30} to any S_1 vibrational description of pDFB[46] in the next section.) The experimental value of the rate coefficient for 6^116^1 therefore may be somewhat high on the basis of these earlier precedents.

Level 6^110^2 is 6-fold degenerate. Parmenter and Tang observe in relaxation from the 6^1 level of benzene that the vibrational excitation process involving the addition of a quantum of ν_{16} (the lowest-frequency vibration) is the most facile deactivation channel.[19] If the addition of ν_{16} is equally facile in relaxation from 6^110^2, then this destination state ($6^110^216^1$) is 12-fold degenerate. We might expect that any treatment of degenerate vibrations may break down for such a degree of degeneracy, especially at the vibrational energies and density of background states that surround the 6^110^2 region. To complicate matters further, level 10^2 displays a large splitting between what are believed to be the two vibrational angular momentum components,[48−50] and the 6^110^2 level will be similarly affected. These strong anharmonic interactions may influence vibrational relaxation rates, as is the case in situations where Fermi resonance interactions are involved. Hence, it is not altogether surprising that the relaxation rate coefficient from this level is substantially different from the rate coefficient calculated on the basis of our model. Nonetheless, even though this level presents the worst case for comparison with the predictions based on our model, the calculation still displays an absolute deviation of <40% from the experimental value.

pDFB: A Case for Exploring Electronic State Dependence (S_0 versus S_1). A direct comparison between vibrational relaxation rates in the S_0 and S_1 states of the same medium-to-large polyatomic molecule was first made for *p*-difluorobenzene by Muller et al. (MLK).[46] The main conclusion from that work was that the vibrational relaxation process was not substantially different in the two electronic states. With the assistance of our model, we can now examine more productively the similarities and/or differences between vibrational relaxation rate coefficients pertaining to the two electronic states.

The calculation of the S_f factors requires a different set of vibrational frequencies for each electronic state, several of which may change markedly from S_0 to S_1. The sensitivity of the S_f factor to the surrounding field of destination states is demonstrated by examining the results of a calculation in which incorrect frequencies are used purposely. The calculation is found to be some 50% astray if the ground-state frequencies are used in place of the excited-state frequencies for estimating the S_1 relaxation rates.

The data sets that we examine are (a) the S_1 pDFB−Ar vibrational relaxation rate coefficients from the work of MLK and subsequently expanded by Catlett et al [51] for the levels ranging from 0^0 to 3^2 ($\epsilon_{vib} = 2500$ cm^{-1}) and (b) data for S_0 pDFB−Ar measured by us previously. These data are compared with predictions obtained using eq 21. We use a hard sphere diameter for the excited electronic state that is 5% larger than for the ground state, in keeping with the 5% increase in the C═C bond length observed in the analogous transition in benzene upon electronic excitation. The observed and predicted rate coefficients for relaxation in both S_0 and S_1 are plotted together against vibrational energy in Figure 4.

From Figure 4, we see that the magnitudes of the estimates of k_i from eq 21 compare quite favorably with the magnitudes observed for vibrational relaxation rate coefficients in both electronic states. This supports the claim that the mechanism of the vibrational relaxation process is not substantially different in the ground and excited electronic states. This should not be entirely unexpected: the hard sphere diameter does not change substantially as a result of electronic excitation for this case (as judged by the small increase in the C═C bond length (∼5%) for benzene). Additionally, from the study of pDFB−Ar van der Waals complexes formed in supersonic free jets, we know

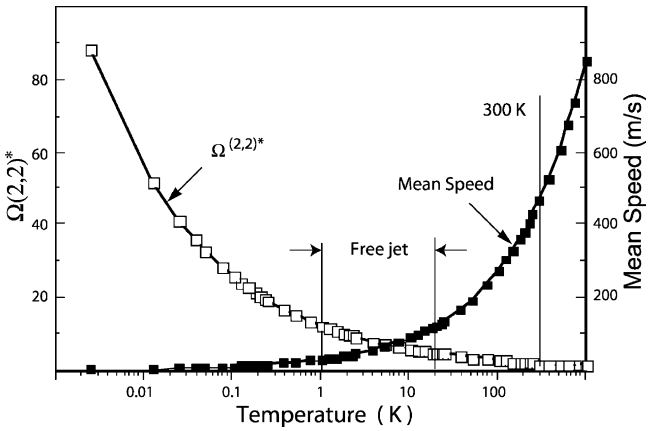

Figure 5. Temperature dependence of the mean speed $\langle v \rangle$ and of the collision integral $\Omega^{(2,2)*}$ in the range of 0.01−1000 K. Regions of interest in this work are indicated. For the purposes of the calculation, the molecular system used was naphthalene−argon (σ_{HS} = 80 Å^2, ϵ_{AM}/k = 261 K; see Supporting Information).

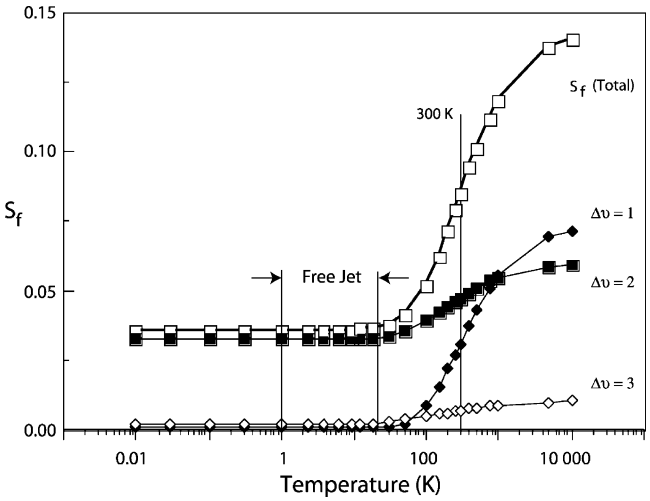

Figure 6. Temperature dependence of the S_f factor. The temperature dependence of each Δv sum of channels is shown explicitly also. At very high and low temperatures, S_f becomes constant.

that the well depth of the pDFB−Ar interaction is only some 30 cm^{-1} deeper in the excited state as compared to that in the ground state.[52] (This is also only a 5% increase.) Of course in systems where there is a substantial structural change induced by electronic excitation, one would expect there to be changes in the vibrational relaxation properties also.

The next striking feature of the comparison shown in Figure 4 is the behavior of the rate coefficient as the energy and character of the initially prepared vibrational level are varied. Particularly obvious is that levels with 1 or more quanta of mode ν_{30} in their description display rate coefficients substantially larger than those that do not contain ν_{30}. This has become known as the "ν_{30} effect". This ν_{30} effect in pDFB (enhancement of the relaxation efficiency by ν_{30}) was identified first for *intra*molecular vibrational redistribution (IVR).[53,54] MLK then demonstrated the influence of ν_{30} in collision-induced relaxation by a comparison of relaxation from the 3^1 and $3^1 30^1$ levels. The ν_{30} effect in both intra- and intermolecular relaxation was the subject of further discussion by Catlett et al.[51] In the case of collision-induced vibrational relaxation, the ν_{30} effect is seen to be entirely rationalized through the calculation of S_f: it is facile in vibrational relaxation because it is a low-frequency mode. In a similar fashion, Whetton and Lawrance[55] have explained the ν_{30} effect in the IVR case.

C. Temperature Dependence of k_i. *Temperature-dependent factors in eq 21.* Our model for estimating vibrational relaxation rate coefficients has been shown to be reliable for a variety of large molecular systems where the target molecule is subjected to collisions by a foreign collision partner at room temperature. In this section, we seek to establish that eq 21 provides a reliable estimate for the absolute magnitude of vibrational relaxation rate coefficients that are observed under conditions of extreme low temperature, such as those offered in a supersonic free jet expansion.

Equation 21 contains a number of factors that are temperature-dependent:

(i) the mean speed $\langle v \rangle$ is directly related to $\sqrt{T}$;

(ii) $\Omega^{(2,2)*}$ contains a complicated temperature dependence as a function of $T^* = kT/\epsilon AM$;

(iii) S_f is temperature-dependent via the Boltzmann factor governing the upward transfer of energy.

The temperature dependence of the mean speed $\langle v \rangle$ and the $\Omega^{(2,2)*}$ integral has been calculated and plotted as a function of temperature from 0.01 to 10 000 K in Figure 5 using data[24] for naphthalene and Ar (Supporting Information). The mean speed is a smoothly increasing function of temperature. The $\Omega^{(2,2)*}$ integral, however, decreases with increasing temperature. The form of the decrease is pseudo-exponential but is not quite regular.

We have calculated S_f probability factors for the same range of temperatures to investigate their temperature dependence. The probability factors are plotted as a function of temperature in Figure 6. The temperature dependence of the S_f factors are determined solely by upward transitions. A lower limit to S_f is formed by the sum of downward propensities, which are not temperature-dependent. There is also an upper limit. At infinite temperature, the Boltzmann distribution is flat. At that point, the propensity would be governed solely by the matrix elements that are analogous to those for downward transfer. The calculations shown in Figure 6 are for naphthalene in the 44^1 level (ϵ_{vib}= 435 cm^{-1}). In the Figure, we have also plotted the temperature dependence of each $|\Delta v|$ group of channels. At low temperature, the dominant contribution to the total S_f arises (for this system at least) from a $|\Delta v| = 2$ channel (because there is insufficient collision energy to access, via a $|\Delta v| = 1$ channel, levels of type 44^1X^1 where ν_x refers to a low-frequency mode and the loss of ν_{44} involves a large ΔE). As the temperature rises, the gain of a single quantum of a low-frequency vibration becomes energetically accessible, and the contribution from upward channels begins to become important. At sufficiently high temperatures, $|\Delta v| = 1$ channels contribute most to the total magnitude of S_f. In general, $|\Delta v| = 2$ channels (involving relatively small ΔE) are most important at very low temperature unless the initial vibrational character contains a low-frequency vibration. In this latter case, $|\Delta v| = 1$ channels may still contribute substantially.

Temperature Dependence between 300 and 5 K. A fairly rigorous test of the temperature dependence and the predictive ability of eq 21 would be obtained for a collision system studied at both room temperature and in the free jet. However, only a few such experimental rate coefficients are available, and none of these are exactly what is required. The experimental data that best facilitate a test of eq 21 are for benzene as the target molecule. Benzene vibrational relaxation data are available for the same vibronic level (6^1) in both the bulb (300 K)[18] and the free jet (<15 K);[56] however, the same collision partner was not used in each instance.

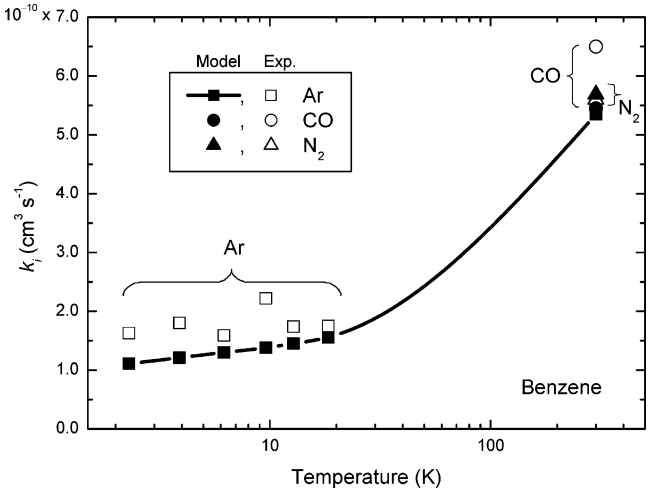

Figure 7. Temperature dependence of k_i over an extended temperature range including the free jet regime and room temperature. The solid guide line joins estimates of k_i (solid symbols) calculated using the model. The free jet data are for benzene−argon;[56] the room-temperature data are for benzene−CO and benzene−N_2.[18]

Benzene vibrational relaxation rate coefficients have been examined in previous sections of this paper to investigate both the collision partner and the vibrational state dependence of the vibrational relaxation process and the ability of eq 21 to estimate the rate coefficients. The data for the 6^1 level in the free jet expansion are available only for Ar as the collision partner. At room temperature, CO and N_2 are the collision partners with the most similar mass and dipole moment. Measurements[19,44] have shown that the rate coefficients for CO and N_2 inducing vibrational relaxation from benzene vibrational levels are similar, both being ∼20% faster than for argon.

Figure 7 shows the experimental rate coefficients for benzene 6^1 deactivation following collision with argon atoms in the low-temperature regime and for collisions with both CO and N_2 at room temperature. Plotted alongside the experimental points is the absolute estimate from eq 21 for benzene−argon collisions. The free jet data lie clustered slightly above the line drawn through the estimated rate coefficients. The temperature dependence is very weak in this region for both the experimental and estimated data. As the temperature increases toward room temperature, the estimated rate coefficient climbs to about 4 times the low-temperature value. The two measured room-temperature rate coefficients for benzene relaxation lie marginally above the predicted room-temperature rate coefficient for argon as a collision partner, but the match is excellent. If reduced masses and well depths for CO or N_2 are used in place of those for Ar, then the estimated rate coefficient is about 5% higher than that estimated for Ar. This Figure displays fairly conclusively that the temperature dependence built into eq 21 via the mean speed, the Ω integral, and the S_f factor reproduces the observed temperature dependence of vibrational relaxation and succeeds in predicting the absolute magnitude of the rate coefficients quite accurately, at least in the temperature regime of $T \leq 300$ K.

D. Comparison of Calculations with a Wide Range of Experimental Data. Figure 8 summarizes the ∼100 calculations of vibrational relaxation rate coefficients from our model that have been made for a variety of molecular systems. The raw data that comprise this Figure are tabulated in Supporting Information. The Figure shows calculated rate coefficients plotted as a function of experimental measurements. Our comments, including an error analysis of the model, follow in the Discussion section.

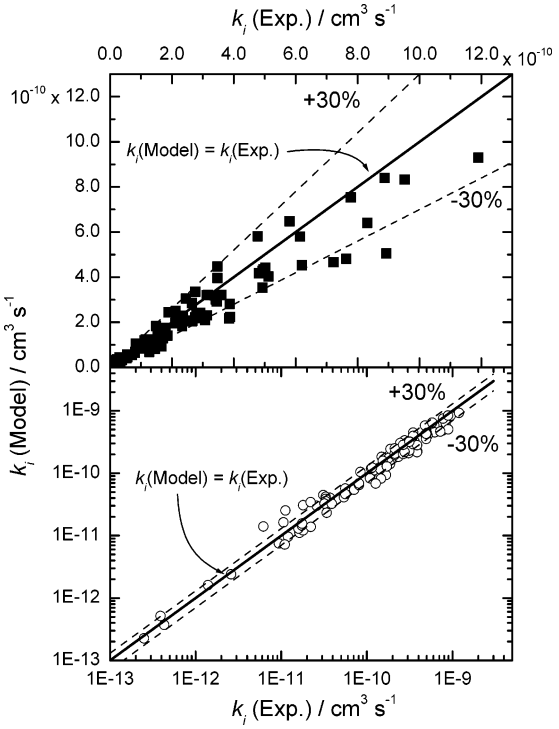

Figure 8. Correlation showing the satisfactory correspondence between observed and estimated k_i values for all of the systems investigated in this work (see Supporting Information). The upper plot uses a linear scale to display the correlation, and the lower plot, a log−log scale. In each case, the solid line through the data represents the identity k_i(exptl) = k_i(model). The two lines astride this line define the ±30% error limits.

IV. Discussion

We have developed a model for estimating vibrational relaxation rate coefficients in molecular systems where vibration to translational (V−T) energy exchange is the dominant mechanism. Varying aspects of the model have been subjected to scrutiny including the vibrational state, electronic state, collision partner, collision energy, and target molecule dependence. In addition, we have monitored the predictive merits of eq 21 with respect to the absolute magnitude of the vibrational relaxation rate coefficient. The equation contains no adjustable parameters, yet it enables the prediction of rate coefficients that span almost 4 orders of magnitude with typically better than 30% accuracy. Given the overall success of the model, we are prompted to discuss a number of its features including

(i) trends in prediction accuracy over the range of molecular systems explored

and

(ii) an extrapolation of various features of the model beyond the limits explored thus far.

In i, we are searching for any trends revealed by an error analysis that might help us interpret the results of our model further. In ii, we extend each feature of the model including temperature, level, and collision partner dependence beyond the limits applied in the experimental data explored here to investigate whether any of these dependencies can be related to those of other models.

A. Error Analysis of the Model. Figure 8 shows calculated rate coefficients plotted as a function of experimental measurements for the range of data tabulated in Supporting Information. There are too many data points to allow individual labeling. All data discussed above are included. Two forms of plots are shown to highlight the accuracy and provide a gauge of the

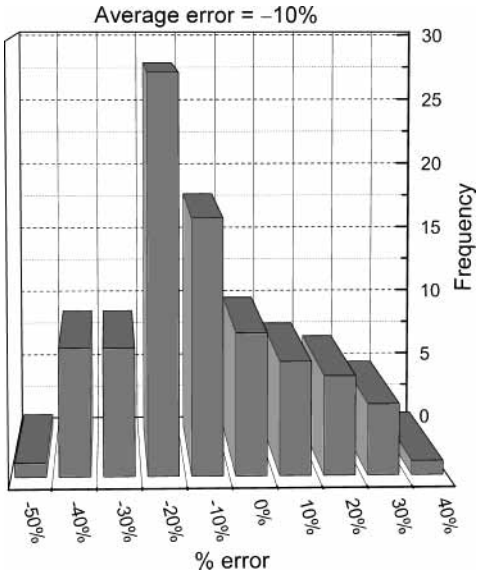

Figure 9. Distribution of errors for the estimation of the vibrational relaxation rate coefficient by the model, derived from the correlation displayed in Figure 8. The average error is −10% (i.e., the model is skewed slightly toward a negative error).

error in the estimated rate coefficients. The upper plot is linear on both axes. A line has been drawn through the data with a slope of unity, representing the relationship k_i(exptl) = k_i(model). Also drawn about this line are two dotted lines representing the ±30% error boundaries. From these boundary lines, it may be seen that most estimates are within ±30% of the experimental values and that aberrant values deviate more often on the negative side of the line.

The lower plot in Figure 8 displays the same information on a log−log scale. This highlights the almost 4 decades of range in the data encompassed in our investigations. Again, the line establishes the equality k_i(exptl) = k_i(model), and the ±30% error lines are now parallel to it. The predictive power of eq 21 is constant over this entire range of data. There is no trend in the percentage error that depends on the magnitude of the estimate.

Figure 9 displays the error in a different form. Errors have been grouped within classes of 10% and plotted as a histogram with frequency. The error distribution is skewed toward negative error, the mean being −10%. These error analyses indicate that eq 21 provides an accurate estimate of k_i within the 4-decades range of relaxation rate data investigated here. The accuracy of the model is typically ±30% across all molecular systems, including small and large polyatomics colliding with a range of collision partners from He to c-hexane with 0 to 3500 cm^{-1} vibrational energy in either the S_1 or S_0 electronic state and with 1 to 200 cm^{-1} average kinetic energy (1−300 K).

B. Limitations of the Model. In previous sections, we have explored the limitations of eq 21 within the range of experimental data available. Limitations have included

(i) the collision partner: the range covered includes atomic, diatomic, and relatively compact polyatomic collision partners (including CO_2, OCS, COF_2, CHF_3, C_2H_4, SF_6, cyclohexane, and pDFB); strongly polar species and extremely "floppy" polyatomics (e.g., long-chain alkanes) are not part of the data set considered;

(ii) the target molecule: when the molecule becomes vibrationally too simple, there may be insufficient averaging over final vibrational states, and hence the average matrix element used in the S_f factors may not be appropriate.

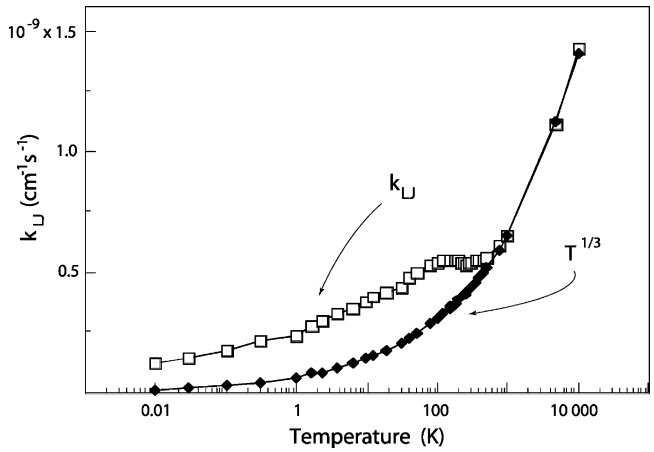

Figure 10. Temperature dependence of the Lennard-Jones elastic rate coefficient k_{LJ} for a wide range of temperatures (system displayed is naphthalene−Ar, (σ_{HS} = 80 Å^2, ϵ_{MM}/k = 261 K; see Supporting Information). At very high temperatures (T > 1000 K), the temperature dependence of k_{LJ} approaches $T^{1/3}$. An inflection is observed in k_{LJ} at temperatures near the magnitude of the well depth.

We now consider the implications of eq 21 further by extending the range of parameters explored thus far and examining how the extremes in these parameters influence the estimated value. We extend the temperature range up to several thousand Kelvin and down to ∼10^{-3} Kelvin. We explore the $\mu^{1/3}$ dependence further. Finally, we examine the S_f factors more closely, including the way in which S_f changes as the density of the background increases still further.

Extremes of Temperature Behavior. In both the very high and very low temperature regimes, the temperature dependence of eq 21 is controlled almost entirely by the Lennard-Jones elastic encounter rate (i.e., at the extremes of temperature, the probability P_{LJ} is essentially temperature-independent; see Figure 6). To investigate the behavior of eq 21 and hence the estimated rate coefficient at high and low temperature, we shall therefore examine the behavior of k_{LJ} in these temperature regimes.

From the theory of inelastic scattering, we expect the rate coefficient for vibrational relaxation to rise sharply at extremely low temperatures because of quantum resonances. The temperature for which such resonance behavior may occur has been a matter of contention.[57−59] However, Schwenke and Truhlar[58,59] predict the onset of such resonance effects to be when the temperature is ∼10^{-3} K, which suggests that the experimental data pertaining to the very low energy collision regime are unlikely to be influenced by quantum resonances. In contrast, some classical theories (e.g., the Landau−Teller theory[11]) have rate coefficients that approach zero at low temperature.

Two competing factors influence the temperature dependence of the Lennard-Jones encounter rate coefficient—the mean speed $\langle v \rangle$ and the Omega integral $\Omega^{(2,2)*}$. It has already been shown that the competition between these two factors satisfactorily explains the observed temperature dependence from room-temperature experiments to experiments performed in supersonic free jets at ∼1−20 K. If the temperature is pushed still further down beyond 1 K, the Ω integral begins to rise quite sharply. In Figure 10, we have plotted the Lennard-Jones rate coefficient k_{LJ} over a large temperature regime for some typical values of the hard sphere cross section (80 Å^2) and well depth (260 K). In the region of T < 1 K, the Lennard-Jones elastic rate has a very flat dependence on temperature—dropping by only ∼40% between 1 and 5 × 10^{-3} K. In this regime, $\Omega^{(2,2)*}$ is a sharply rising function of temperature.

As the temperature extends substantially beyond room temperature, the dependence of k_i is again found to be controlled almost solely by k_{LJ}. As we extend the plot in Figure 10, k_{LJ} continues to rise. To examine the functional form of the temperature dependence at very high temperature, we have plotted the correlation between $T^{1/3}$ and T alongside k_{LJ}. It may be seen clearly that at temperatures above ~1000 K the functional form of the k_{LJ} temperature dependence approaches $T^{1/3}$. $\langle v \rangle$, of course, is dependent on $T^{1/2}$; $\Omega^{(2,2)*}$ reduces this to $T^{1/3}$. Temperature-dependent factors related to $T^{1/3}$ appear regularly in classical theories of vibrational relaxation at these temperatures.[4] The classical theories have been more successful in describing the temperature dependence of k_i in this high-temperature regime. Indeed, the Landau−Teller repulsive interaction model[11] provides a temperature dependence for the relaxation rate that is dependent on $T^{1/3}$. SSH theory has a similar temperature dependence;[13] $\log(P)$ is related to $-T^{-1/3}$. We would not necessarily have expected that our model, described by eq 21, held true well above room temperature. However, it is pleasing to find that our model does, in fact, display a temperature dependence in this high-temperature regime that is consistent with many existing theories.

Influence of the Collision Partner. The dependence on the collision partner that has been built into eq 21 is probably the weakest link in the model. The true dependence of k_i on the collision partner is both varied and complex. Certainly any function based solely on reduced mass, in whatever form, cannot be expected to reproduce the observed dependence on the collision partner well. We have ignored entirely all polar collision partners (except molecules with only small permanent dipoles such as CO). For dipolar molecules, an interaction between the permanent dipole of the collision partners and either the quadrupole or an induced dipole in the target molecule means that the Lennard-Jones (6, 12) potential around which we have built our model does not necessarily portray adequately the true intermolecular potential. Additionally, we have rejected data relating to relaxation with vibrationally complex collision partners (e.g., alkyl chains). In those cases, the opportunity for resonance-enhanced V−V processes becomes significant, and the model is not able to cover such cases.

Even within these constraints, however, there are still complications that are revealed by the experimental data. Data for the noble gases (rigorously V−T only and zero permanent dipole moment) provide some points for discussion. SSH theory and many experimental results for diatomic relaxation actually provide a probability for relaxation P that decreases with increasing mass of the collision partner.[13] For larger polyatomics, as we have seen, the dependence is quite the reverse. There are some data provided by Steinfeld on iodine relaxation[60] in which both are observed to occur; an increasing P with reduced mass when the mass is small, followed by a leveling off and a decrease with reduced mass for larger masses. The turning point for iodine−M relaxation is at a collision partner mass of about 50 amu. For different molecules, the turning point is seen to move. For OCS−M collisions, P rises from M = H_2 and M = He but then has diminished substantially for M = Ar.[61] An interpretation of this effect is a resonance between the velocity of the incoming molecule and the vibrational frequency of the target molecule.[62] As the velocity (dictated of course by the mass of the molecule) decreases (i.e., mass increases), it may move into and then out of resonance with the vibrational frequency of the target molecule. For a higher vibrational frequency, then, it is reasonable that the turning point (or resonance mass) moves to lower mass (higher velocity). This is what has been observed for I_2 and OCS, with iodine having a vibrational frequency of ~100 cm^{-1}, and OCS, ~520 cm^{-1}. For diatomics with higher vibrational frequencies, it is possible that the resonance may never be reached, all collision partners being too heavy. Therefore, only a decreasing propensity with collision-reduced mass would be observed, as is predicted by SSH theory.

Further insight into this effect might be obtained in measurements of state-to-state propensities where the different channels provide a different amount of vibrational energy exchange for the same collision partner. The environment of the supersonic free jet may also assist in unravelling this issue by providing a much slower collision partner for the same mass. Velocities can be changed routinely by a factor of 3−4 (a temperature change of a factor of 15) whereas at higher temperatures this is substantially more difficult to achieve.

In our development of the model, the estimation of $I(\Delta E)$ was simplified to differentiate only between exoergic and endoergic transfer processes (eqs 15 and 16). Because our objective has been to develop a simple model for estimating state-to-*field* rate coefficients that uses no adjustable parameters, we have expressly excluded a consideration of a collision partner-sensitive $I(\Delta E)$. This embellishment might be warranted (indeed desirable) for a model designed to evaluate state-to-*state* propensities. However, the heavy final-state averaging that occurs in our state-to-*field* model means that a collision partner-dependent $I(\Delta E)$ is an unwarranted complication given that the model works satisfactorily in its absence.

Influence of Vibrational-Level Structure. The S_f factors are one of the most important components in our semiempirical model of vibrational relaxation. They are the dominant factor in scaling the magnitude of the estimate provided by eq 21. The dependence of S_f on the vibrational state reproduces in both a relative and absolute sense the observed vibrational-state dependence in most cases. We build on the success of our calculations of S_f and make some further comments concerning the vibrational relaxation process.

The overriding influence in determining k_i from eq 21 comes from S_f, which is in turn dominated by the exponential energy gap behavior of the matrix element. The falloff of the exponential is set somewhat arbitrarily as $-0.01\Delta E$ and was chosen by Parmenter and Tang[13] on the basis of some results of SSH theory. (See also Yardley.[4]) The factor of 10 that was chosen to distinguish $|\langle 0|Q|1\rangle|^2$ from $|\langle 0|Q|2\rangle|^2$ is also somewhat arbitrary and is based on the typical magnitude of $\Delta v = 1$ and $\Delta v = 2$ propensities observed in mode-to-mode studies in just a few systems.[60,61] We believe that the success of S_f is entwined in the averaging that is carried out by summing the propensities for all destination states. However, even when the number of normal modes is relatively small, S_f often provides a reasonable estimate for k_i. What is surprising is the generality and consistency of the size of the matrix elements that have been used across a large variety of molecular systems.

We turn our attention to the behavior of S_f in regions where the density of background vibrational states becomes very high. The highest background density of states explored thus far is ~200 vibrational states/cm^{-1} in S_0 pDFB. As the density of states rises and the description of the initial state becomes more complex, so too will the S_f factor rise. For the higher levels studied in pDFB, the relaxation rate was found to be approximately the Lennard-Jones elastic encounter rate. We question whether the vibrational relaxation rate coefficient will continue to rise with S_f or whether some upper bound be reached, for example, some inelastic rate coefficient calculated with a

more precise intermolecular potential. Evidence from work on pDFB indicates that some upper bound may be reached.[30] This upper bound may not be the Lennard-Jones elastic rate; however, it probably lies close to it.

V. Summary

We have proposed a simple semiempirical, semiclassical model to estimate the rates of vibrational relaxation for a wide variety of molecular systems. The model is based on calculating an efficiency P for the vibrational relaxation process. The vibrational relaxation rate coefficient is calculated as the product of P and the classical Lennard-Jones elastic encounter rate. The probability is dependent on a calculation that carries out a summation of a set of mode-to-mode propensities. The probability is also taken to be dependent on the cube root of the reduced mass of the collision pair. There are no adjustable parameters. The calculated vibrational relaxation rate coefficients using the model have been compared to a variety of experimentally obtained rate coefficients involving more than 10 molecules colliding with a variety of collision partners at temperatures from 1 to 300 K. The accuracy of the calculated rate coefficients has been found to be within about ±30% for these rate coefficients, which span 4 orders of magnitude. We have concentrated on larger collision systems because the approximations inherent in the model are more likely to be valid; accordingly, we have not by any means covered all of the work that has been performed on vibrational relaxation, particularly for small molecules. We have examined much of the available large-molecule data (pertaining to low−intermediate state density), but much of the substantial database relating to vibrational relaxation in small molecules has not been explored. We have tried to model systems that demonstrate different facets of the vibrational relaxation process and provide explicit tests on how our model performs. En route, we have explored systems with target molecules up to large aromatics, both ground and excited electronic states, collision partners from helium to cyclohexane, and initial vibrational levels from 1 to 100 quanta, 0 to 10 000 cm^{-1} of energy, and densities of destination states from 1/500 cm^{-1} to 500/cm^{-1}.

Of course all models have their qualifications. Our interpretation of probability $P = S_f \times \mu^{1/3}$ does not include additional factors such as steric effects, dipole moments, other intermolecular potentials, and so forth. Theories for particular molecules have been developed to include these factors. It is plausible that total rates of deactivation, as opposed to state-to-state rates, because of the inherent averaging, are less sensitive to individual variations caused by these factors. Despite these qualifications, we feel that our model provides a simple and effective method for estimating absolute V−T vibrational relaxation rates for a wide variety of systems.

Acknowledgment. Financial support from The Australian Research Council as well as from Griffith and Sydney Universities is gratefully acknowledged. Support from the U.S.−Australia Bilateral scheme has also been seminal in permitting collaborations over the years between members of the Molecular Dynamics Laboratory (Griffith University) and our U.S. colleagues including Professor Jeffrey Steinfeld (MIT), Professor Joe Francisco (Purdue), and of course Professor Charles Parmenter (Indiana). We are particularly indebted to the Fulbright Foundation for supporting a visit to Griffith University by Professor Parmenter in 1980 at a time when S.H.K. was very much in the formative stages of his career. Indeed, the foundation of this paper was developed in the Ph.D. thesis of S.H.K.[28] The work has drawn some of its inspiration from the insights and experimental creativity of the contributions made to the field of large-molecule vibrational relaxation by Professor Charlie Parmenter over some 3 decades. The opportunity to participate in an edition of this journal commemorating Professor Parmenter's 70th birthday was a very welcome stimulation for us to get together and present this theory formally and, in doing so, pay tribute to a member of the physical chemistry community whose influence has touched us so deeply. Both A.E.W.K. and S.H.K. have relished deeply the numerous collegiate and personal interactions we have been privileged to enjoy with Charlie Parmenter.

Supporting Information Available: A tabulation is available of the experimentally determined rate coefficients for state-to-field vibrational relaxation used in the comparisons between theory and experiment (presented graphically in this paper as Figure 8). The data include measurements from many laboratories for a range of target molecules and a wide variety of collision partners. This material is available free of charge via the Internet at http://pubs.acs.org.

References and Notes

(1) Parmenter, C. S. *J. Phys. Chem*. **1982**, *86*, 1735.
(2) Krajnovich, D. J.; Parmenter, C. S.; Catlett, D. L., Jr. *Chem. Rev.* **1987**, *87*, 237
(3) Weitz, E.; Flynn, G. W. *Annu. Rev. Phys. Chem.* **1984**, *25*, 275. Weitz, E.; Flynn, G. W. *Adv. Chem. Phys* **1981**, *47*, 185.
(4) Yardley, J. T. *Introduction to Molecular Energy Transfer*; Academic Press: New York, 1980.
(5) Tardy, D. C.; Rabinovich, B. S. *Chem. Rev.* **1977**, *77*, 369.
(6) Oref, I.; Tardy, D. C. *Chem. Rev.* **1990**, *90*, 1407.
(7) Quack, M.; Troe, J. *Int. Rev. Phys. Chem.* **1981**, *1*, 97.
(8) Weston, R. E., Jr.; Flynn, G. W. *Annu. Rev. Phys. Chem.* **1992**, *43*, 559.
(9) Barker, J. R.; Toselli, B. M. *Int. Rev. Phys. Chem.* **1993**, *12*, 305.
(10) Flynn, G. W.; Parmenter, C. S.; Wodke, A. M. *J. Phys. Chem.* **1996**, *100*, 12817.
(11) Landau, L.; Teller, E. *Phys. Z.* **1936**, *10*, 34.
(12) Tanczos, F. I. *J. Chem. Phys*. **1956**, *25*, 439.
(13) Schwartz, R. N.; Slawsky, Z. I.; Herzfield, K. F. *J. Chem. Phys.* **1952**, *20*, 1591.
(14) Child, M. S. *Molecular Collision Theory*; Academic Press: New York, 1974.
(15) Gilbert, R. G.; Smith, S. C. *Theory of Unimolecular and Recombination Reactions*; Oxford University Press: Oxford, England, 1990.
(16) Barker, J. R. *Ber. Bunsen-Ges. Phys. Chem.* **1997**, *101*, 566.
(17) Clary, D. C. *J. Phys. Chem*. **1987**, *91*, 1718.
(18) Tang, K. Y.; Parmenter, C. S. *J. Chem. Phys.* **1983**, *78*, 3922.
(19) Parmenter, C. S.; Tang, K. Y. *Chem. Phys.* **1978**, *27*, 127.
(20) Chernoff, D. A.; Rice, S. A. *Chem. Phys.* **1979**, *70*, 2521.
(21) Vandersall, S. A.; Chernoff, D. A.; Rice, S. A. *J. Chem. Phys.* **1981**, *74*, 4888.
(22) McDonald, D. B.; Rice, S. A. *J. Chem. Phys.* **1981**, *74*, 4907.
(23) Catlett, D. L., Jr.; Parmenter, C. S.; Pursell, C. J. *J. Phys. Chem.* **1994**, *98*, 3263.
(24) Muller, D. J.; McKay, R. I.; Kable, S. H.; Lawrance, W. D.; Edwards, G. B.; Hardy, J. P.; Rock, A. B.; Selway, K. R.; Knight, A. E. W. *J. Phys. Chem*. **1988**, *92*, 3751.
(25) Kable, S. H.; Knight, A. E. W. *J. Chem. Phys.* **1987**, *86*, 4709.
(26) Catlett, D. L., Jr.; Parmenter, C. S.; Pursell, C. J. *J. Phys. Chem.* **1995**, *99*, 737.
(27) Lin, H. M.; Seaver, M.; Tang, K. Y.; Knight, A. E. W.; Parmenter, C. S. *J. Chem. Phys.* **1979**, *70*, 5442.
(28) Kable, S. H. Ph.D. Thesis, Griffith University, Australia, 1988.
(29) Thoman, J. W., Jr.; Kable, S. H.; Rock, A. B.; Knight, A. E. W. *J. Chem. Phys.* **1986**, *85*, 6234.
(30) Kable, S. H.; Thoman, J. W., Jr.; Knight, A. E. W. *J. Chem. Phys.* **1988**, *88*, 4748.
(31) Stone, T. A.; Parmenter, C. S. *J. Phys. Chem. A* **2002**, *106*, 938.
(32) Barker, J. R. *J. Phys. Chem.* **1985**, *88*, 11.
(33) Hartland, G. V.; Qin, D.; Dai, H.-L.; Chen, C. J. *J. Chem. Phys.* **1997**, *107*, 2890.
(34) Troe, J. *J. Chem. Phys.* **1977**, *66*, 4758.
(35) Lenzer, T.; Luther, K.; Troe, J.; Gilbert, R. G.; Lim, K. F. *J. Chem. Phys.* **1995**, *103*, 626.

(36) Wright, S. M. A.; Sims, I. R.; Smith, I. W. M. *J. Phys. Chem. A* **2000**, *104*, 10347.
(37) Damm, M.; Hippler, H.; Troe, J. *J. Chem. Phys.* **1988**, *88*, 3564.
(38) Bernshtein, V.; Oref, I. *J. Chem. Phys.* **1998**, *108*, 3543.
(39) Sevy, E. T.; Michaels, C. A.; Tapalian, H. C.; Flynn, G. W. *J. Chem. Phys.* **2000**, *112*, 5844.
(40) Kohlmaier, G. H.; Rabinovich, B. S. *J. Chem. Phys.* **1963**, *38*, 1692.
(41) Hirschfelder, J. O.; Curtiss, C. F.; Bird, R. B. *Molecular Theory of Gases and Liquids*, 2nd ed.; Wiley: New York, 1964.
(42) Miclavc, A.; Fischer, S. *Chem. Phys. Lett.* **1976**, *44*, 209. Miclavc, A.; Fischer, S. *J. Chem. Phys.* **1978**, *69*, 281.
(43) Wilson, E. B.; Decius, J. C.; Cross, P. C. *Molecular Vibrations*; McGraw-Hill: New York, 1955.
(44) Logan, L. M.; Buduls, I.; Knight, A. E. W.; Ross, I. G. *J. Chem. Phys.* **1980**, *72*, 5667.
(45) Atkinson, G. H.; Parmenter, C. S.; Tang, K. Y. *J. Chem. Phys.* **1979**, *71*, 68.
(46) Muller, D. J.; Lawrance, W. D.; Knight, A. E. W. *J. Phys. Chem.* **1984**, *87*, 4952.
(47) McDonald, D. B.; Rice, S. A. *J. Chem. Phys.* **1981**, *74*, 4918.
(48) Knight, A. E. W.; Parmenter, C. S.; Schuyler, M. W. *J. Am. Chem. Soc.* **1975**, *97*, 1993. Knight, A. E. W.; Parmenter, C. S.; Schuyler, M. W. *J. Am. Chem. Soc.* **1975**, *97*, 2005.
(49) Callomon, J. H.; Dunn, T. M.; Mills, I. M. *Philos. Trans. R. Soc. London, Ser. A* **1966**, *259*, 499.
(50) Fischer, G.; Knight, A. E. W. *Chem. Phys.* **1992**, *168*, 211.
(51) Catlett, D. L., Jr.; Holtzclaw, K. W.; Krajnovich, D.; Moss, D. B.; Parmenter, C. S.; Lawrance, W. D.; Knight, A. E. W. *J. Phys. Chem.* **1985**, *89*, 1577.
(52) Butz, K. W.; Catlett, D. L., Jr.; Ewing, G. E.; Krajnovich, D.; Parmenter, C. S. *J. Phys. Chem.* **1986**, *90*, 3533.
(53) Kable, S. H.; Lawrance, W. D.; Knight, A. E. W. *J. Phys. Chem.* **1982**, *86*, 1244.
(54) Fujii, M.; Ebata, T.; Mikami, N.; Ito, M.; Kable, S. H.; Lawrance, W. D.; Parsons, T. B.; Knight, A. E. W. *J. Phys. Chem.* **1984**, *88*, 2937.
(55) Lawrance, W. D.; Whetten, N. *J. Phys. Chem.* **1993**, *93*, 5385.
(56) Muller, D. J. Ph.D. Thesis, Griffith University, Australia, 1988.
(57) Van Zoeren, C.; Rock, A. B.; Kable, S. H.; Edwards G. B.; Knight, A. E. W. *J. Chem. Phys.* **1988**, *89*, 6777.
(58) Schwenke, D. W.; Truhlar, D. G. *J. Chem. Phys.* **1984**, *81*, 5586.
(59) Schwenke, D. W.; Truhlar, D. G. *J. Chem. Phys.* **1985**, *83*, 3454.
(60) Steinfeld, J. I.; Klemperer, W. *J. Chem. Phys.* **1965**, *42*, 3475.
(61) Smith, N. J. G.; Davis, C. C.; Smith, I. W. M. *J. Chem. Phys.* **1984**, *80*, 6122.
(62) Rapp D.; Kassel, T. *Chem. Rev.* **1969**, *69*, 61.